

Flexural behavior of RC beams retrofitted by ultra-high performance fiber-reinforced concrete

Leila Meraji^a, Hasan Afshin* and Karim Abedi^b

Department of Civil Engineering, Sahand University of Technology, P.O. Box 51335-1996, Tabriz, Iran

(Received September 25, 2018, Revised April 26, 2019, Accepted June 17, 2019)

Abstract. This paper presents an investigation into the flexural behavior of reinforced concrete (RC) beams retrofitted by ultra-high performance fiber-reinforced concrete (UHPFRC) layers. The experimental study has been conducted in two parts. In the first part, four methods of retrofitting with UHPFRC layers in both the up and down sides of the beams have been proposed and their efficiency in the bonding of the normal concrete and ultra-high performance fiber-reinforced concrete has been discussed. The results showed that using the grooving method and the pre-casted UHPFRC layers in comparison with the sandblasting method and the cast-in-place UHPFRC layers leads to increase the load carrying capacity and the energy absorption capacity and causes high bond strength between two concretes. In the second part of the experimental study, the tests have been conducted on the beams with single UHPFRC layer in the down side and in the up side, using the effective retrofitting method chosen from the first part. The results are compared with those of non-retrofitted beam and the results of the first part of experimental study. The results showed that the retrofitted beam with two UHPFRC layers in the up and down sides has the highest energy absorption and load carrying capacity. A finite element analysis was applied to prediction the flexural behavior of the composite beams. A good agreement was achieved between the finite element and experimental results. Finally, a parametric study was carried out on full-scale retrofitted beams. The results indicated that in all retrofitted beams with UHPFRC in single and two sides, increasing of the UHPFRC layer thickness causes the load carrying capacity to be increased. Also, increases of the normal concrete compressive strength improved the cracking load of the beams.

Keywords: ultra-high performance fiber-reinforced concrete; retrofitted beams; bonding surface; load carrying capacity; energy absorption capacity; numerical analysis

1. Introduction

An effective technique for the retrofitting of existing concrete elements in order to increase their resistance and durability is adding ultra-high performance fiber-reinforced concrete (UHPFRC) layers to the existing elements. UHPFRC was characterized by high binder content, very low water-to-cement ratio (w/c), use of silica fume, fine quartz powder and superplasticizer and fibers (Richard and Cheyrezy 1995, Cheyrezy *et al.* 1995). Many studies conducted on mechanical properties of UHPFRC (Roux *et al.* 1996, Bonneau *et al.* 1997, Chan and Chu 2004, Cwirzen *et al.* 2008, Lai and sun 2010, Yazici *et al.* 2010, Wille *et al.* 2011b, Garas *et al.* 2012, Tam *et al.* 2012, Wang *et al.* 2012, Yazıcı *et al.* 2013, Zheng *et al.* 2013, Zong *et al.* 2014, Shi *et al.* 2015, Nematzadeh and Poorhosein 2017) have shown superior properties of this material. UHPFRC has a compressive strength more than 150 MPa, with high packing density, high durability, increased energy absorption

capacity, improved resistance against freeze-thaw cycles and high penetration resistance.

Adding fibers improved tensile strength and ductility of UHPFRC, considerably (Skazlic´ and Bjegovic´ 2009, William *et al.* 2010, Wille *et al.* 2011a, Zheng *et al.* 2013, Graybeal and Baby 2013, Rahdar and Ghalehnovi 2016). Because of these properties, UHPFRC is a promising material to improve structural resistance and durability of damaged concrete structures.

It has been found that by increasing fiber volume ratio from 0% to 5%, the tensile strength of UHPFRC increased linearly (Kang *et al.* 2010). The increased amount of fibers decreased the workability and the mechanical performance of the mixture (Dupont and Vandewalle 2005). Combination of two or three different fibers was used to minimize the amounts of fiber and achieve desired performance (Qian and Stroeven 2000, Park *et al.* 2012). The effects of combinations of micro and macro fibers on the flexural performance of UHPFRC were studied by Kim *et al.* (2011). They found that energy absorption capacity and deflection capacity with combination 1.0% micro and 1.0% macro fibers were 45.4-75.9% and 48.7-67.9% greater than those with 2.0% microfibers, respectively. Poorhosein and Nematzadeh (2018) studied the effects of adding steel fibers, PVA fibers, and their combination on the properties of UHPFRC. They concluded that a considerable improvement (42%) was achieved in the tensile strength of the specimen contained hybrid fibers of 0.75% steel and

*Corresponding author, Associate Professor

E-mail: hafshin@sut.ac.ir

^aPh.D. Student

E-mail: L_meraji@sut.ac.ir

^bProfessor

E-mail: k_abedi@sut.ac.ir

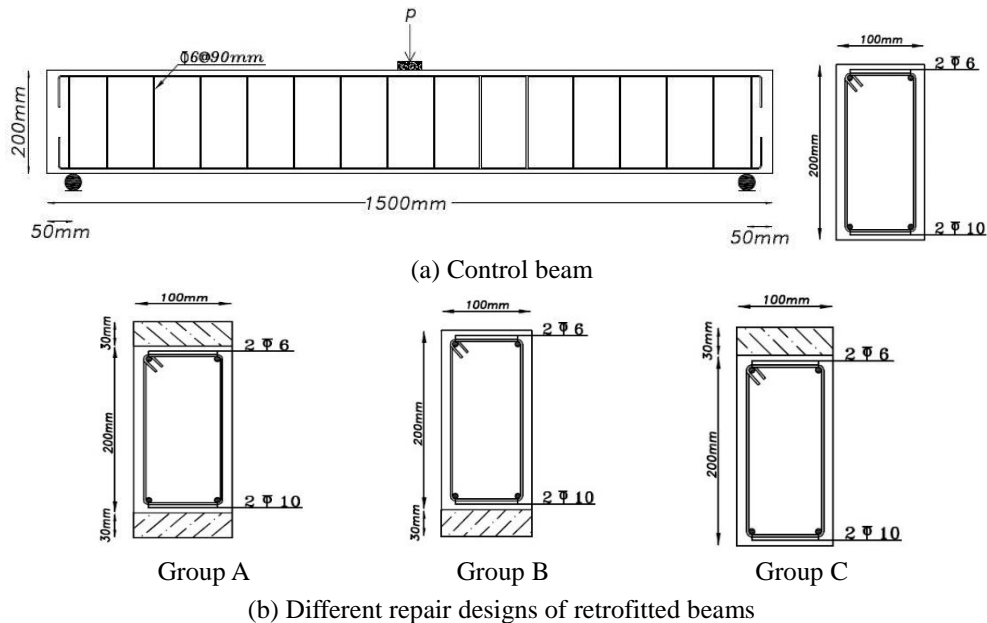


Fig. 1 Details of beams

0.25% PVA fibers. Moreover, PVA fibers had a negligible effect on the tensile strength of UHPFRC.

In some researches, UHPFRC is used for shear and torsional strengthening of beams (Jandaghi Alaei and Karihaloo 2003, Mohammed *et al.* 2015a, b). Also, there are some studies on flexural strengthening of beams with additional UHPFRC layers. Habel *et al.* (2007) and Noshiravani and Brühwiler (2013) investigated the effects of the combination of UHPFRC with reinforcing steel bars in reinforced concrete beams. They proposed this method as a promising way to strengthen existing concrete beams. Hussein and Amleh (2015) carried out experimental studies on composite prisms and beams without stirrups, having UHPFRC layer in the tension side. The test results indicated that the performance of the proposed composite system, in terms of flexural and shear capacity, was successfully improved. Lampropoulos *et al.* (2016) conducted extensive numerical modeling on beams strengthened with additional layer of UHPFRC in the compressive side, in the tensile side and also with three sides UHPFRC jackets. The main conclusion of this study is that the beam with three sides UHPFRC jackets achieved superior performance. Safdar *et al.* (2016) studied the flexural behavior of reinforced concrete beams retrofitted in tension and compression zone, with UHPFRC of varying thicknesses. Experimental and analytical results showed that the ultimate flexural strength of RC beams, retrofitted in tension and compression zone, was enhanced with the increase of UHPFRC thickness. Al-Osta *et al.* (2017) used UHPFRC layers in three various configurations to strengthen RC beams. The highest load carrying capacity increase was obtained from the beam strengthened on three sides (bottom and two longitudinal sides) and the lowest increase in load carrying capacity was obtained from the beam strengthened only at the bottom side. Tanarlan (2017) and Tanarlan *et al.* (2017) studied RC beams behaviors strengthened in the tensile side with prefabricated UHPFRC laminates using two different

bonding approaches: gluing with epoxy and mechanical anchoring. The experimental results revealed that adding UHPFRC laminates, especially in the case of anchorage, is an effective way to enhance the load carrying capacity. The load carrying capacity increased up to 208% in some cases. Murthy *et al.* (2018) used some analytical models for prediction of flexural behavior of reinforced concrete beams retrofitted with UHPFRC. They showed that the predicted values of ultimate load and numbers of cycles to failure are in good agreement with the experimental results.

This research is focused on the addition of UHPFRC layers to reinforced concrete (RC) beams. Since the important parameter for the response of retrofitted elements is the interface between normal concrete and UHPFRC layer, one of the main objectives of this study is to investigate into the bonding behavior of the UHPFRC layer with the existing beams in order to improve the interface performance. Moreover, UHPFRC layers were added in the top side, bottom side and both top and bottom sides of RC beams and the efficiency of using them for retrofitting of the beams have been studied. Thereafter, a parametric study was conducted to examine the influence of UHPFRC layer thickness and normal concrete compressive strength.

2. Methods and materials

2.1 Specimen characteristics

In order to investigate into the structural behavior of retrofitted beams, seven reinforced concrete beams were constructed and tested under three-point flexural loading up to failure. The beams have a length of 1500 mm and cross section of 100 mm×200 mm. Fig. 1(a) shows the details of the control beam as the non-retrofitted beam. The stirrups with 6 mm diameter were placed at 90 mm spacing to prevent shear failure. Two reinforcing bars with 10 mm

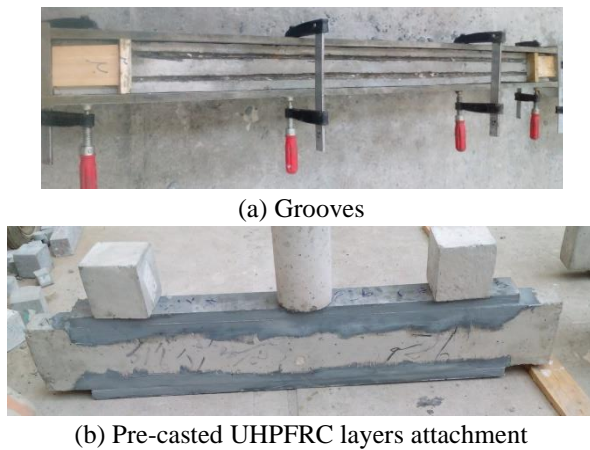


Fig. 2 Grooves and pre-casted UHPFRC layers attachment

diameter were used as tensile reinforcement and two 6 mm bars as compressive reinforcement in all beams with the concrete cover thickness of 15 mm. Fig. 1(b) illustrates the cross section of three different retrofitted specimens. The UHPFRC layer thickness of 30 mm was used for retrofitting of the beams. As shown in Fig. 1(b), retrofitted beams were classified into 3 groups. Group A consisted of four beams retrofitted by the UHPFRC layers in each up and down sides. Group B and C consisted of one specimen, retrofitted by the single layer of UHPFRC in up and down sides, respectively.

The experimental program for this study is as follows: At first, four methods of bonding the UHPFRC layer with normal concrete were used for each beam in group A and the behavior of retrofitted beams was examined and the effective method opted. Then, by choosing the effective method of bonding, the beams in groups B and C were prepared and their behavior was compared with those of the control beam and the beam in group A prepared using the same method.

The four retrofitting methods were implemented are as follows:

- 1) Two longitudinal grooves with a length of 1240 mm and width and depth of 10 mm were cut on the beam surfaces of the up and down sides (Fig. 2(a)). The grooves were cleaned with an air jet. Then, the layer of epoxy was used on the surfaces of the beam and filled the grooves too. The pre-casted UHPFRC layers (with 30 mm thickness) adhered to the surfaces (Fig. 2(b)). The extra epoxy was removed.
- 2) Two longitudinal grooves were applied on the beam surfaces like above. Then, the UHPFRC layer with 30 mm thickness was cast in two sides (cast-in-place layers).
- 3) The surface of two sides of the concrete beam was sandblasted until the aggregates were apparent (Fig. 3(a)). Then the dust and dirt were removed by the air jet and a layer of epoxy covered the surfaces. Then the pre-casted UHPFRC layers were directly applied to the surfaces.
- 4) Two sides of the concrete beam were sandblasted until the aggregates were apparent and then UHPFRC layers were cast on the surfaces (Fig. 3(b)).

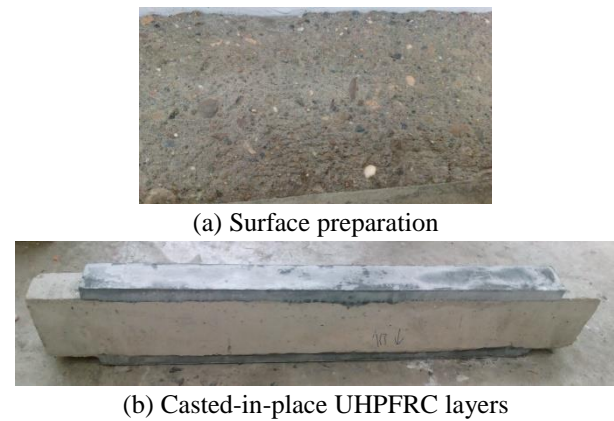


Fig. 3 Surface preparation and casted-in-place UHPFRC layers

Table 1 The Specifications of the tested beams

Group	Beam	Repair location	Method of surface preparation	Type of UHPFRC layer
	Control	No repair		
A	UD-GP	Up and down	Grooving method	Pre-casted layer
	UD-SP	Up and down	Sandblasting method	Pre-casted layer
	UD-GC	Up and down	Grooving method	Cast-in-place layer
	UD-SC	Up and down	Sandblasting method	Cast-in-place layer
B	D-GP	Down	Grooving method	Pre-casted layer
C	U-GP	Up	Grooving method	Pre-casted layer

Table 1 gives the specifications of the experimental beams in 3 groups of A, B and C. The specimen nomenclature is as follows: the first letters before (-) refer to the location of repairing (up or down). The next letter after (-) indicates the method of preparing of beam surfaces (making grooves or sandblasting). The following letter indicates the type of used UHPFRC layers in the specimen (pre-casted or cast-in-place UHPFRC layer). For example, specimen UD-GP is a specimen that grooves were made in two up and down sides and then the pre-casted UHPFRC layers connected to the beam by epoxy.

2.2 Materials

In UHPFRC matrix, the used cement was a type II Portland Cement and its chemical compositions are as follows:

$$C_3S = 45 \text{ percent, } C_2S = 32 \text{ percent, } C_3A = 0 \text{ percent and } C_4AF = 14 \text{ percent.}$$

The used silica fume had the fineness of about 20000 m²/kg and its carbon content was approximately 0.3 percent. Its SiO₂ content was usually greater than 90 percent. The quartz sand had a maximum grain size of 700 μm and with SiO₂ content between 85 to 90 percent. The used quartz powders had SiO₂ content about 99 percent and

Table 2 The mix compositions of UHPFRC and the normal concretes (kg/m³)

Concrete type	Cement	Silica fume	Quartz powder	Quartz sand	Superplasticizer	Water	Fibers (in vol.)	Course aggregate	Fine aggregate
UHPFRC	850	195	145	860	41	192	2%		
Normal concrete	365					180		900	925

Table 3 The properties of the epoxy adhesive

Density (kg/l)	Tensile strength (MPa)	Tensile modulus (MPa)	Flexural modulus (MPa)
1.31	30	4500	3800

the average diameter of its particles was 10 μm . The suitable workability of the concrete was ensured by the use of a superplasticizer based on polycarboxylate ether. Its specific gravity and PH were 1.12 and 7, respectively. The end hooked steel fibers (20 mm length and 0.35 mm in diameter) with a tensile strength of above 2000 MPa were used (in 2% volume fraction). The mix compositions of UHPFRC and the normal concrete are given in Table 2.

As before mentioned, each specimen was reinforced with 10 and 6 mm diameter reinforcing bars. The yield strength of 10 and 6 mm diameter bars was 400 and 300 MPa, respectively. Also, the properties of two-component epoxy adhesive used in the current study according to the manufacturer's catalog are represented in Table 3.

2.3 Specimens preparation method

The RC beams with normal concrete were demolded just one day after casting and their surfaces were roughened with methods of sandblasting or making grooves. The beams were cured under standard condition. After 28 days, in beams with cast-in place UHPFRC layers, a UHPFRC layer was cast over the RC beams. Then after another 48 hours, the UHPFRC layer of the lower part of the beams was also cast. The cast-in-place UHPFRC layers were demolded after 48 hours. When the casting of these retrofitted beams was completed, they were standard cured for 28 days.

In beams with pre-casted UHPFRC layers, after 28-day standard curing of the RC beams and the pre-casted UHPFRC layers, the UHPFRC layers were adhered to the up and down regions of the beams using an epoxy adhesive. Then the retrofitted beams were kept in the laboratory until the test day.

2.4 Mechanical properties of concretes

To characterize UHPFRC and normal concrete, the uniaxial compressive and tensile strength tests were conducted according to ASTM C39 and ASTM C496. These properties are usable in the finite element model. The compressive strength of UHPFRC and normal concrete after 28 days was obtained 125 and 32 MPa, respectively and the tensile strength was found about 7 and 3 MPa, respectively. The uniaxial compressive and tensile behavior for the normal concrete and UHPFRC are presented in Fig. 4 and Fig. 5.

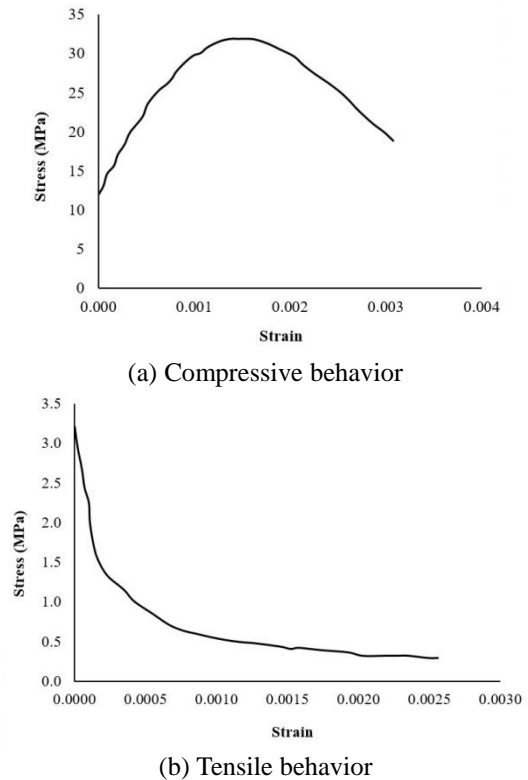


Fig. 4 The properties of the normal concrete

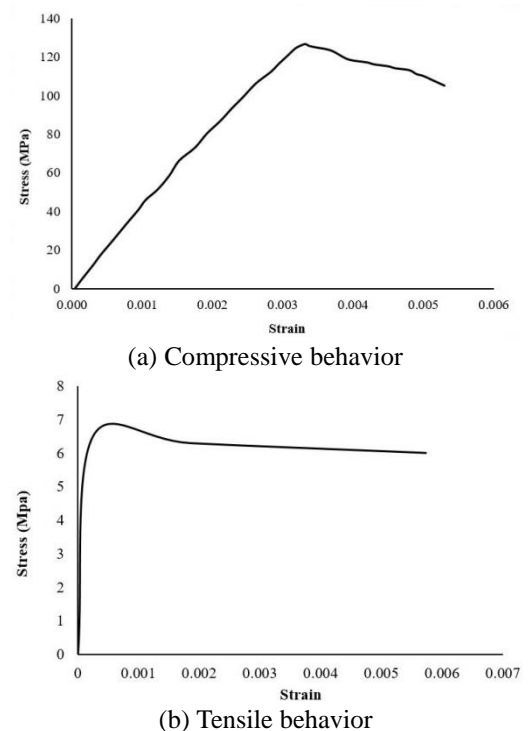


Fig. 5 The properties of UHPFRC



Fig. 6 The Loading setup

2.5 Loading setup

The tests were conducted under the displacement control condition. A concentrated load was applied at the mid-span and a load cell of 100 KN capacity was used. In order to measure the displacement, a linear variable differential transducer (LVDT) was installed under the loading point at the mid-span of the beams. Fig. 6 illustrates the loading setup.

3. Results and discussion

3.1 Bending behavior of the retrofitted beams by two UHPFRC layers with four retrofitting methods (group A)

As mentioned before, four methods of retrofitting were used for the beams in group A. The bending behaviors of the beams are evaluated in order to find the most appropriate and effective method.

3.1.1 Failure modes and crack patterns

The behavior of all four beams in group A was typical flexural. The failure patterns are illustrated in Fig. 7 for the specimens. The first visible crack was observed on the UHPFRC layer in the bottom side of the beams and some flexural cracks were appeared in the middle of the beams. By continuing in the loading, the cracks tend to open and several flexural cracks were also propagated at the concrete beams. Also, the previously occurred crack in the UHPFRC layer progressively started to widen, but because of the strong bonding between two concretes, horizontal shear cracks were occurred and the cracks tried to split the normal concrete cover below the level of the tensile reinforcement. Then, yielding of the tensile reinforcement and increasing the cracks width cause the failure to be occurred.

Considering the behavior of the specimens with the cast-in-place UHPFRC layers (UD-SC and UD-GC), debonding between normal concrete and UHPFRC was occurred in UD-GC (Figs. 7(a) and 7(b)). It means that the sandblasting method causes more roughened surfaces and therefore best bonding between two concretes was observed. However, debonding is not occurred in the specimens with the pre-casted layers (UD-SP and UD-GP) due to the presence of the epoxy resin (Figs. 7(c) and 7(d)).

3.1.2 Load carrying capacity



(a) UD-SC



(b) UD-GC



(c) UD-SP



(d) UD-GP

Fig. 7 Failure modes and crack patterns of the beams in group A

• Effect of using the grooving and sandblasting methods:

Fig. 8 illustrates the load-displacement responses of the beams retrofitted by four methods. Table 4 presents the results of the tests. According to Table 4, in the retrofitted specimens with pre-casted UHPFRC layers and using epoxy, the maximum load carrying capacity of 65 KN was obtained for UD-GP specimen in comparison with that of UD-SP specimen with the maximum load of 60.4 KN (7.6% increase). Furthermore, in the retrofitted specimens with the cast-in-place UHPFRC layers, maximum load carrying capacity of 59 KN was obtained for UD-GC specimen, which shows a 2.2% increase with respect to UD-SC specimen (57.7 KN).

A comparison between the grooving and sandblasting methods revealed that in the grooving method, the load carrying capacity enhanced slightly due to the increase in the bonding surface.

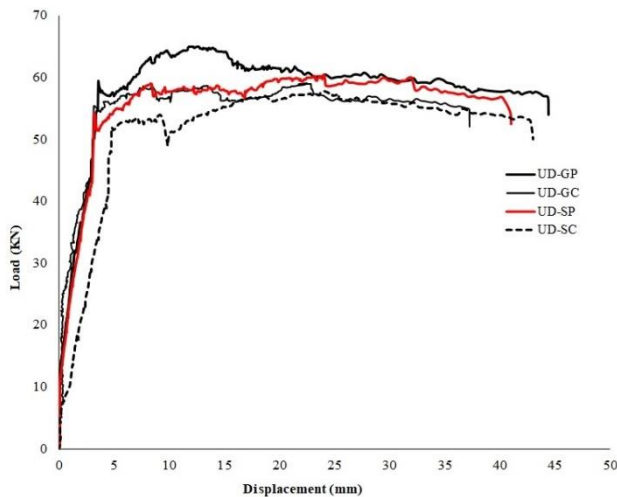


Fig. 8 Load-displacement responses of the beams in group A

Table 4 Results of the beam specimens in group A

Specimen	Maximum load carrying capacity (KN)	Energy absorption capacity (KN.mm)
UD-GP	65	2602
UD-GC	59	2042
UD-SP	60.4	2243
UD-SC	57.7	2200

• *Effect of using of the pre-casted and cast-in-place UHPFRC layers:*

As a comparison between the test results in the specimens with pre-casted and cast-in-place UHPFRC layers, it is observed that the maximum load carrying capacity of UD-GP specimen was 65 KN which is 10% greater than that of UD-GC (59 KN). Also, a 5% increase was observed in the maximum load carrying capacity of UD-SP specimen in comparison with that of UD-SC specimen.

Using the pre-casted UHPFRC layers enhanced the maximum load carrying capacity of the beams slightly. Because the bonding strength of the interface, using epoxy resin, was higher.

3.1.3 Energy absorption capacity

The area under the load-displacement curves up to the failure point is computed as the energy absorption capacity of the beam specimens. The energy absorption capacity for the specimens in group A is calculated and presented in Table 4. Considering the energy absorption capacity of the retrofitted specimens by the methods of grooving and sandblasting, it is observed that the amount of the energy absorption capacity of UD-GP is 16% higher than that of the UD-SP specimen and in UD-GC, this amount is 93% of the UD-SC specimen. In the comparison of the results for the specimens with the cast-in-place and pre-casted UHPFRC layers, the energy absorption capacity of UD-SP is nearly equal to that of UD-SC and in UD-GP is 27% higher than that of UD-GC.

According to the obtained results, because of increasing the maximum load carrying capacity and the energy

absorption capacity by using the grooving method and the pre-casted UHPFRC layers and good bonding between two concretes, this method (method 1) was selected as an appropriate and effective method for preparing the rest of the beams (in group B and C) in the second part of the study.

3.2 The comparison of the bending behavior of the retrofitted beams with single UHPFRC layer (groups B and C), the beam with two UHPFRC layers (group A) and the control beam:

In this part of the study, beams with UHPFRC layers in just the down and the up side were prepared and their behaviors were obtained and compared with those of the control beam and UD-GP specimen (the beam with the UHPFRC layers in two sides).

3.2.1 Failure modes and crack pattern

The failure modes and crack patterns for the specimens with single and double UHPFRC layers and the control beam are illustrated in Fig. 9. All the beams are failed in the flexural behavior.

The control beam and U-GP specimen showed the same cracking pattern. At the lower loads, no cracks appeared. As the load increased, there were more flexural cracks spread in the middle span. After increasing the amount of applied load, the cracks began to extend to the compressive zone, their width increased and some diagonal cracks appeared in the shear span. Finally, in the control beam, some compressive cracks and concrete crushing was observed in the compressive zone. However, in the U-GP specimen, all cracks were flexural and no crushing was observed in UHPFRC. In U-GP specimen, failure occurred at about 53 KN which is 1.5 times higher than that of the control beam with failure load of 35 KN.

D-GP and UD-GP specimens behaved in a same flexural manner. In the D-GP specimen, the tensile strain was increased due to the presence of the UHPFRC layer in the down side. Therefore, the first visible crack occurred in the UHPFRC layer at the bottom of the beam. In the UD-GP specimen, due to the presence of the UHPFRC layer in two sides, the strain was increased in both sides. The first visible crack started from the UHPFRC layer in the down side. By increasing the applied load, more flexural cracks appeared in the middle of the beams, tending to open. On further loading, flexural cracks propagated to the loading point in the compressive side, and the cracks width was expanded. Finally, the D-GP and UD-GP specimens failed at the load levels of 40 and 56 KN, respectively, which is 1.14 and 1.6 times more than the failure load of the control beam. In the D-GP specimen, concrete crushing occurred in the compression side. No debonding was observed between the normal concrete and the UHPFRC layer in the retrofitted beams.

3.2.2 Load carrying capacity

Fig. 10 illustrates the mid-span displacement of the D-GP, U-GP, UD-GP specimens and the control beam versus the applied loads. The figure shows that before the initiation of the tensile cracks, the initial stiffness of all the retrofitted

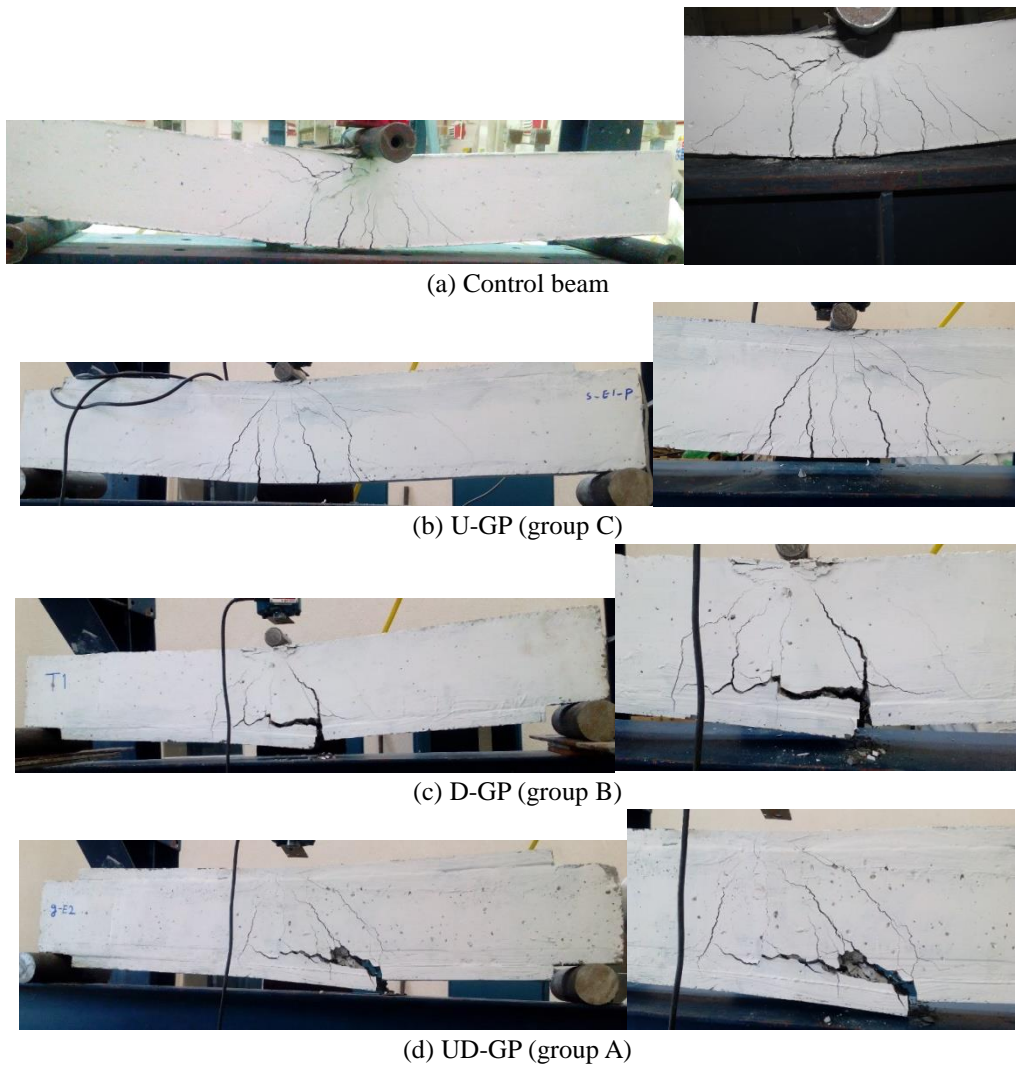


Fig. 9 Failure modes and crack patterns of the beams

beams and the control beam are the same. It means that before the beginning of the cracks, the loads were carried by the normal concrete in the retrofitted beams. In the load-displacement curves of all retrofitted beams, after the appearance of cracks, at first the stiffness decreases and then it increases. It is due to the high stiffness of the UHPFRC layers and their increasing contribution to the load carrying capacity of the specimens. Also, increasing of the stiffness has been influenced by the retrofitting methods, that is, the beam retrofitted by the UHPFRC layers in two sides demonstrated stiffer behavior than the retrofitted beams by single UHPFRC layer.

The values of the maximum load carrying capacity of all the specimens in this part of the study are presented in Table 5. It can be seen that the maximum load carrying capacity of the specimen retrofitted by two UHPFRC layers in the up and down sides, the UD-GP specimen, has increased 56% compared to that of the control beam. This increase is 27% and 10% for the U-GP and D-GP specimens, having single UHPFRC layer in the up side and the down side, respectively.

In comparing the behaviors of the D-GP, U-GP and UD-GP specimens with together, it can be observed that the

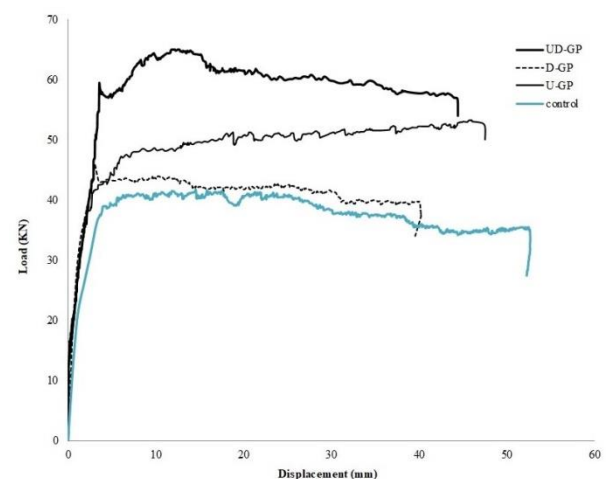


Fig. 10 Load-displacement responses of the beams in all groups

maximum load carrying capacity of the UD-GP specimen has increased 41% with respect to D-GP, however, there is a 22% increase in maximum load carrying capacity of the UD-GP respect to U-GP. In the U-GP specimen, having

Table 5 Results of the beam specimens in all groups

Specimen	Maximum load carrying capacity (KN)	Increase in maximum load carrying capacity (%), compared to the control beam	Energy absorption capacity (KN.mm)	Increase in energy absorption capacity (%), compared to the control beam
UD-GP	65	+56	2602	+50
D-GP	46	+10	1765	+2
U-GP	53.2	+27	2303	+33
Control	41.7	-	1731	-

UHPFRC layer in the up side, 15% increase is observed compared to that of the D-GP specimen.

3.2.3 Energy absorption capacity

The energy absorption capacity of the specimens of D-GP, U-GP, UD-GP and the control specimen is calculated and presented in Table 5. The energy absorption capacity increased considerably in the specimens retrofitted by the UHPFRC layer in the up side (UD-GP and U-GP) compared to the control beam. The increasing amount in the UD-GP and U-GP specimens is 50% and 33%, respectively. In the D-GP specimen, retrofitted in the down side, the energy absorption capacity increased slightly (2%).

According to Table 5, the energy absorption capacity of the UD-GP and U-GP specimens is 1.47 and 1.30 times higher than that of the D-GP specimen. Moreover, the energy absorption capacity of the UD-GP and U-GP specimens is nearly equal.

4. Numerical analysis

4.1 Verification

A numerical analysis carried out to verify the flexural behavior of the tested beams. For the finite element analysis, ABAQUS software was used. Numerical analyses were carried out for the control beam and the beams retrofitted in the down side, in the up side and two sides.

The compressive and tensile behavior of the normal concrete and UHPFRC was modeled based on the experimental results as shown in Fig. 4 and Fig. 5. The elastic modulus of UHPFRC and the normal concrete was regarded to be 42 and 25 GPa, respectively and the poisson ratio of both concretes was assumed 0.17.

The behavior of steel rebars in tension was modeled with a linear elasto-plastic model. The elastic modulus and poisson ratio of steel are regarded as 210 GPa and 0.3.

For simulation of normal concrete and UHPFRC, a C3D8R element as a 3-D stress 8-noded linear brick element was used and the steel reinforcing bars and stirrups were simulated with a T3D2 element as a 2-noded linear 3-D truss element. The numerical model is illustrated in Fig. 11. For simulation of the nonlinear behavior of normal concrete and UHPFRC, concrete damage plasticity model (CDPM) was used in the finite element analysis. The used parameters in CDPM are including: ψ (the dilation angle), ζ (the eccentricity parameter), σ_{b0}/σ_{c0} (the ratio of biaxial

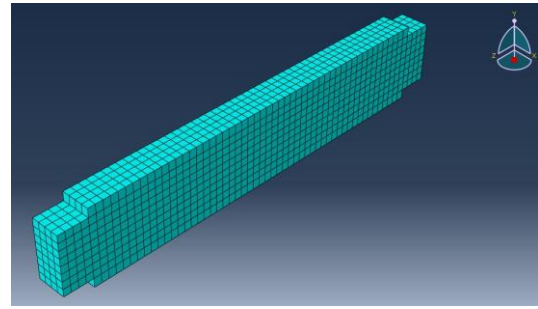


Fig. 11 The numerical model of the retrofitted beam in two sides

Table 6 Parameters used in the concrete damage plasticity model

	ψ	ζ	σ_{b0}/σ_{c0}	k_c	μ
Normal concrete	36	0.1	1.16	0.666	0.0001
UHPFRC	36	0.1	1.16	0.666	0.0001

compressive strength to uniaxial compressive strength), k_c is used to define the shape of the failure surface in deviatoric plane which is the ratio between distances measured from the hydrostatic axis to tensile and compressive meridians and μ is the viscosity parameter. These parameters are presented in Table 6. Because no debonding was observed in the interface, the bonding between normal concrete and UHPFRC was assumed perfect. This assumption was also considered in many other studies regarding the behavior of repaired beams with concrete jackets. For example, in the study performed by Safdar *et al.* (2016), high-pressure water-jet was used to expose the aggregate of concrete surface after one day of casting of the beams. Then UHPFRC was poured on the rough surface and there was high bond strength in the interface. Al-Osta *et al.* (2017) applied two methods of using epoxy adhesive to bond UHPFRC strips on concrete beams and pouring UHPFRC on sandblasted surfaces. Ramachandra Murthy *et al.* (2018) used epoxy adhesive to bond the UHPFRC strips to the rough surface of the beams and these cause strong bonding during the test. Safdar *et al.*, Al-Osta *et al.* and Ramachandra Murthy *et al.* assumed the perfect bonding between two concretes and their finite element modeling was in a good agreement with experimental results.

The load-displacement response of the experimental and numerical models is presented in Fig. 12. It can be seen that the numerical results are in good agreement with the experimental results.

Fig. 13 shows the tensile crack pattern at the failure point for all specimens. The numerical models show the same crack pattern as the experimental models. It can be seen that in the numerical models, there are not any considerable tensile cracks in the UHPFRC layers, especially in the upside layers (Fig 13(b), Fig 13(c) and Fig 13(d)).

4.2 parametric study

A parametric study was carried out for the beams

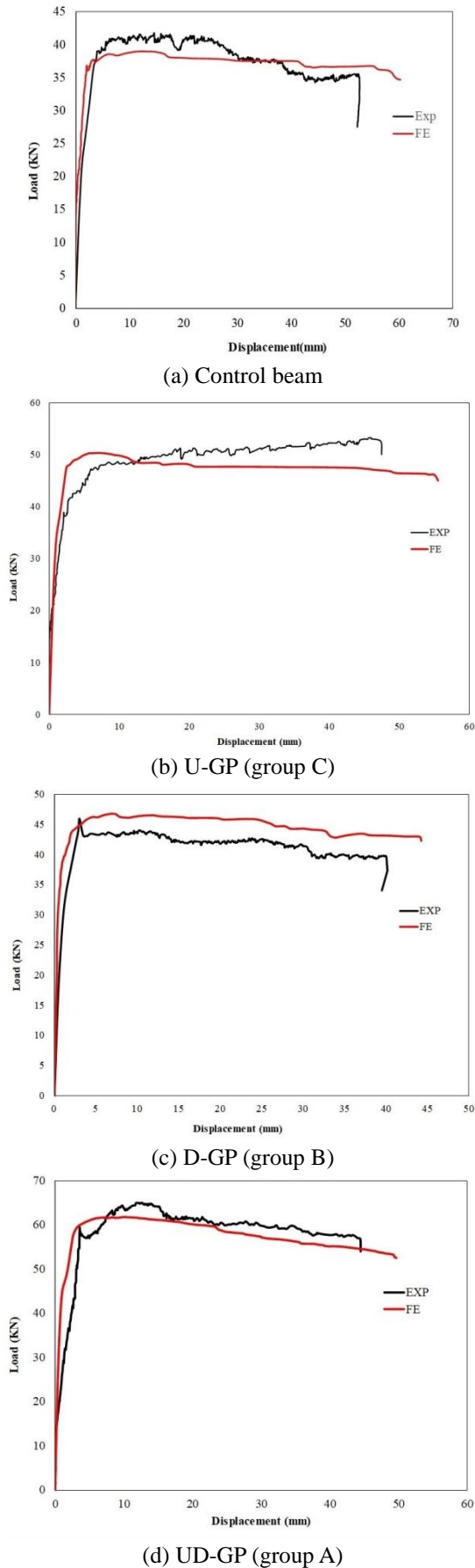


Fig. 12 Load-displacement response of the experimental and numerical models

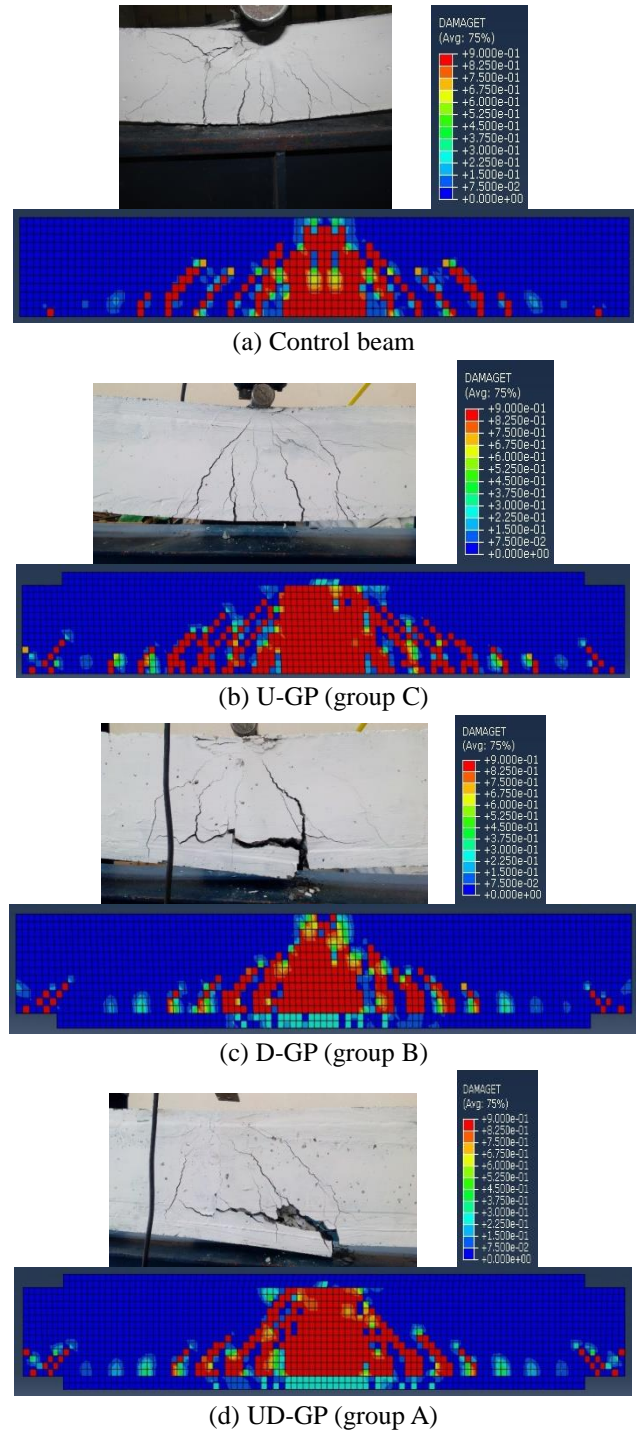


Fig. 13 Tensile crack pattern of all specimens

retrofitted in the bottom side, in the up side and in the both sides. The influence of the thickness of the UHPFRC layer and compressive strength of the normal concrete were examined. The parametric study was conducted for a typically sized beam with details as shown in Fig. 14. The properties used for materials in the parametric study are the same as those of the verified models in the last section.

4.2.1 Influence of the thickness of the UHPFRC layer

The thickness of the UHPFRC layer is an important parameter that affects the behavior of the retrofitted beams.

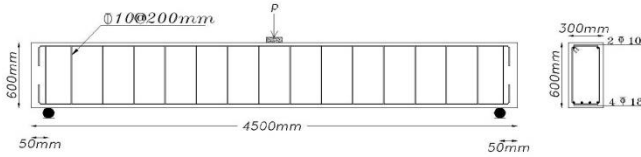
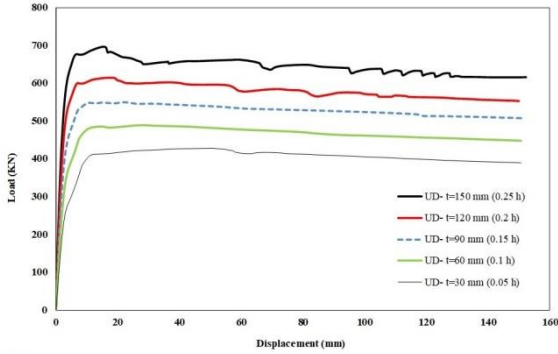
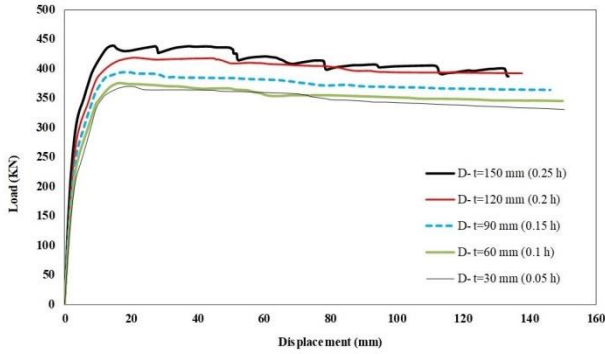


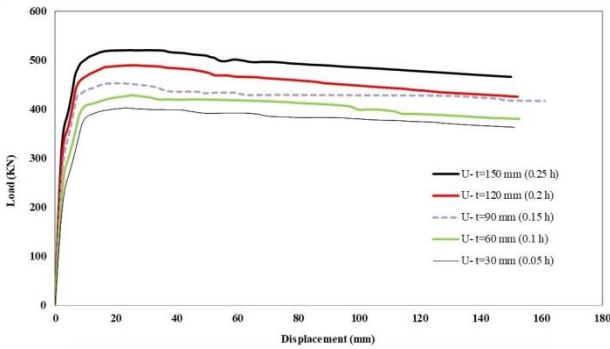
Fig. 14 Details of the typically sized beam in the parametric study



(a) Retrofitted beams in two sides (group A)



(b) Retrofitted beams in the down side (group B)



(d) Retrofitted beams in the up side (group C)

Fig. 15 Load-deflection curves for the retrofitted beams with various thicknesses of the UHPFRC layer

In the present study, five different thicknesses for the UHPFRC layer were considered as $t=30, 60, 90, 120$ and 150 mm. The ratios of these values to the height of the control beam (h) are: $t/h=0.05, 0.1, 0.15, 0.2$ and 0.25 , respectively.

The effect of the thickness of the UHPFRC layer on the load-deflection responses of the retrofitted beams in bottom, in top and in the both sides are shown in Fig. 15. Also, the relation of the maximum load carrying capacity with the thickness of UHPFRC layer is illustrated in Fig. 16. Based

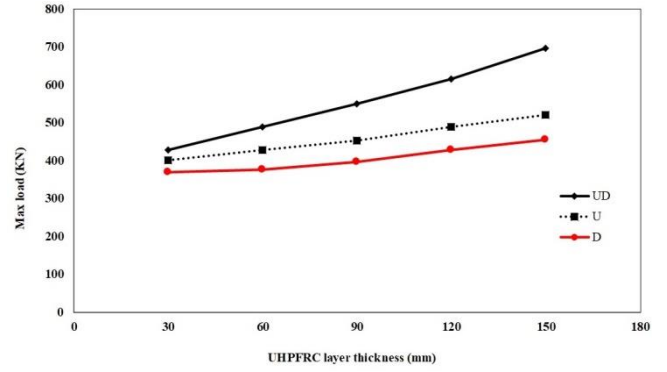


Fig. 16 The relation of the maximum load carrying capacity for the retrofitted beams with various UHPFRC layer thickness values

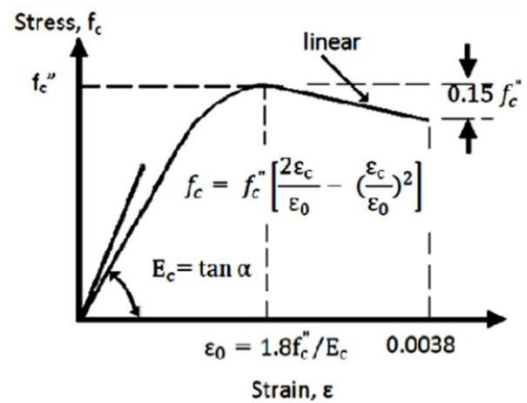


Fig. 17 Modified Hognestad curve for the estimation of the concrete compressive behavior

on the results of Fig. 15, increasing of the UHPFRC layer thickness leads to the increase of stiffness in the all groups of beams. Also, the load carrying capacity of the all retrofitted beams was increased. This is because of the high strength and strain hardening of UHPFRC. The highest increase value of the maximum load compared to that of the control beam (351 KN) belongs to the retrofitted beams in the both sides. The maximum loads in UD, U and D-specimens with 150mm UHPFRC layer are 1.98, 1.48 and 1.30 times higher than that of the control beam, respectively.

According to Fig. 16, in the both specimens retrofitted in single side, in each 0.05 increase in t/h , an increasing value of 6% on average was observed in the maximum load carrying capacity. The respective increasing value for retrofitted beams in two sides was higher and equal to 12%.

4.2.2 Influence of the compressive strength of the normal concrete

In this part of the study, the used uniaxial compressive stress-strain relationship for the normal concrete is obtained by using the concrete curve proposed by Hognestad (1951) (Fig. 17 and Eqs. (1)-(2)).

$$f_c = f_c'' \left[\frac{2\varepsilon_c}{\varepsilon_0} - \left(\frac{\varepsilon_c}{\varepsilon_0} \right)^2 \right] \quad (1)$$

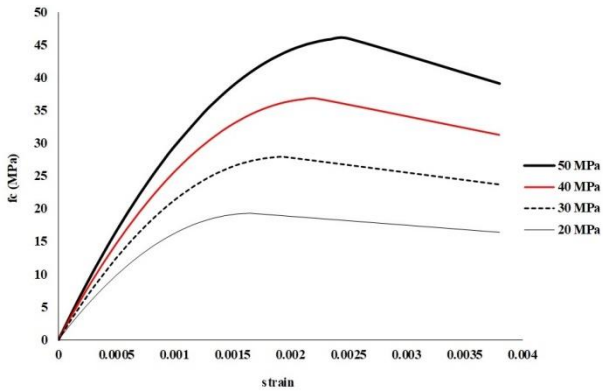


Fig. 18 Stress-strain curves for normal concrete with various compressive strength values

$$f_c'' = k_s f_c' \quad (2)$$

The concrete strain, ε_0 , corresponds to the maximum stress, f_c'' . For concretes with compressive strength (f_c') of 15 MPa, 20 MPa, 25 MPa, 30 MPa and equal or more than 35 MPa, k_s is considered as 1, 0.97, 0.95, 0.93 and 0.92, respectively. The descending branch of Hognestad curve in Fig. 17 is began from point of (f_c'' , ε_0) to the point of (f_c'' , $0.85 \varepsilon_0$). The crushing strain, ε_u , is taken as 0.0038.

The uniaxial tensile strength of the normal concretes was measured using Eq. (3), according to ACI 318-14

$$f_t = 0.56 \sqrt{f_c'} \quad (3)$$

In the tension zone, the behavior of the concrete is linear before reaching to the maximum tensile strength, f_t , or before cracking. After cracking, the reduced stress is reached to a strain corresponding to 10 times of cracking strain.

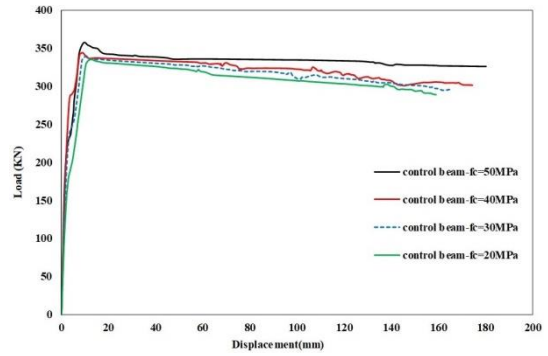
The modulus of elasticity of the normal concretes was calculated using Eq. (4), according to ACI 318-14

$$E_c = 4700 \sqrt{f_c'} \quad (4)$$

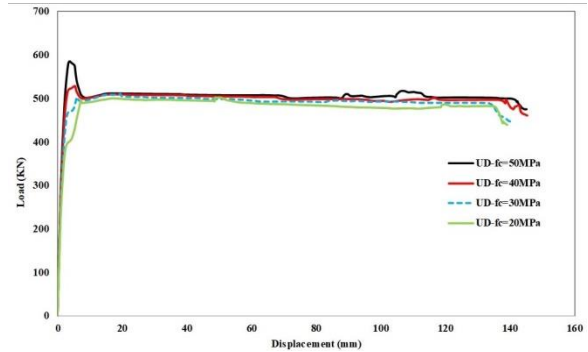
For the normal concrete compressive strength, four values were assumed as 20 MPa, 30 MPa, 40 MPa and 50 MPa. The obtained compressive stress-strain relationships are illustrated in Fig. 18.

The numerical analysis was carried out for all retrofitted beams as well as control beam. Fig. 19 illustrates the load-deflection curves of the specimens. Fig. 20(a) shows the relation of the maximum load carrying capacity of the beams with different normal concrete compressive strength values. It can be seen that varying of f_c' has no significant effect on the maximum load carrying capacity of the beams. Fig. 20(b) shows the relation of the values of cracking load with different normal concrete compressive strength values. The results demonstrate that adding UHPFRC layers in all groups of retrofitted beams causes the delaying of the cracking, especially in the beams retrofitted in the both sides, that is, by increasing of f_c' , cracking load is increased.

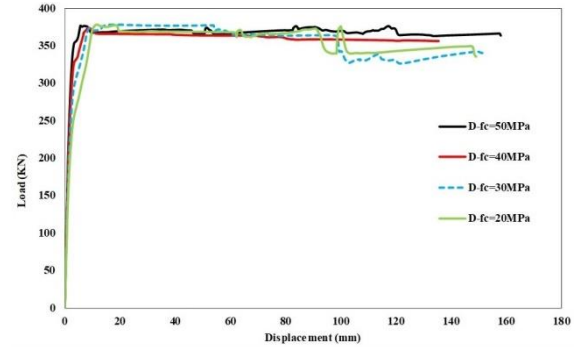
5. Conclusions



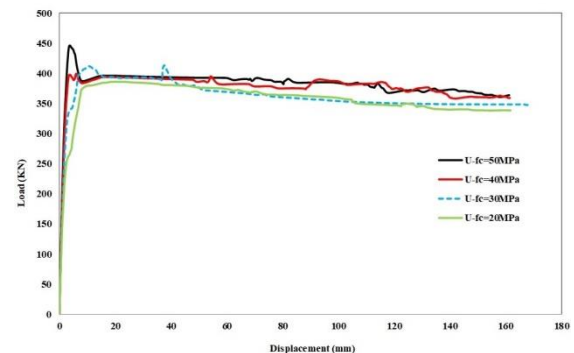
(a) Control beams



(b) Retrofitted beams in two sides (group A)



(c) Retrofitted beams in the down side (group B)



(d) Retrofitted beams in the up side (group C)

Fig. 19 Load-deflection curves for the beams with various values of the normal concrete compressive strength

In the present paper, an investigation into the flexural behavior of reinforced concrete (RC) beams retrofitted by ultra-high performance fiber-reinforced concrete (UHPFRC) layers has been carried out. In the first part of the study, the efficiency of the four proposed retrofitting methods was investigated. To do this, four reinforced concrete beams,

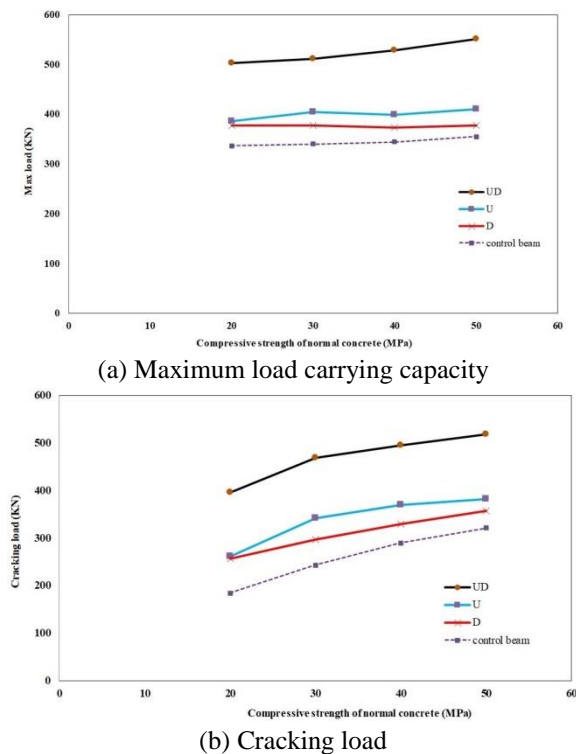


Fig. 20 The relation of the maximum load carrying capacity and the cracking load with various values of the normal concrete compressive strength

retrofitted by two UHPFRC layers in the up and down sides, were tested. In the second part, by using the most appropriate and effective retrofitting method, the beams with single UHPFRC layer in the down side and the up side were cast and their behaviors were examined. According to the current study, the following conclusions can be drawn:

- The first part of the study: (Comparison of the four retrofitting methods in group A)

1) In comparing the grooving and the sandblasting methods in the retrofitted beams, the load carrying capacity increased about 5% on average when the grooving method was used. Also, by using the pre-casted UHPFRC layers in the retrofitted beams, the maximum load carrying capacity increased 7.5% on average compared to the use of the cast-in-place UHPFRC layers. So, using the grooving method and the heat-treated pre-casted UHPFRC layers provided a slight increased load carrying capacity.

2) The beam prepared by using the grooving method and the pre-casted UHPFRC layers had the highest energy absorption capacity.

3) No debonding was observed between the normal concrete and the UHPFRC layer when the pre-casted UHPFRC layer and the grooving method was used.

- The second part of the study: (Comparison of the retrofitted beams with single and double UHPFRC layers)

1) Using the UHPFRC layer in both the up and down sides led to the higher increasing amount of the load carrying capacity (56%), in comparison with the control beam. In the beam retrofitted in the up side, the

maximum load carrying capacity increased about 27% and the increasing amount was 10% for the beam retrofitted in the down side.

2) For the beams retrofitted in two sides and the up side, the increasing amount of the energy absorption capacity was about 50% and 33%, respectively compared to the control beam. The energy absorption capacity of the beam with the single UHPFRC layer in the down side increased slightly (2%).

- A numerical model was developed to prediction of the structural behavior of the retrofitted beams using concrete damage plasticity model. The numerical results were agreed well with experimental data.

- The parametric study reveals that the increase of the UHPFRC layer thickness causes the load carrying capacity of the beams retrofitted in the down side, in the up side and in the both sides, to be increased. Furthermore, by increasing of the normal concrete compressive strength, the cracking load of the mentioned specimens increased.

References

- ABAQUS Analysis User's Manual (2014), Version 6.14, Dassault Systems Simulia Corp., Providence, RI, USA.
- ACI 318M-14 (2014), Building Code Requirements for Structural Concrete and Commentary, American Concrete Institute, Farmington Hills, MI, USA.
- Al-Osta, M.A., Isa, M.N., Baluch, M.H. and Rahman, M.K. (2017), "Flexural behavior of reinforced concrete beams strengthened with ultra-high performance fiber reinforced concrete", *Constr. Build. Mater.*, **134**, 279-296. <https://doi.org/10.1016/j.conbuildmat.2016.12.094>.
- ASTM C39 (2015), Standard Test Method for Compressive Strength of Cylindrical Concrete Specimens, ASTM International, West Conshohocken, PA, USA.
- ASTM C496 (2011), Standard Test Method for Splitting Tensile Strength of Cylindrical Concrete Specimens, ASTM International, West Conshohocken, PA, USA.
- Bonneau, O., Lachemi, M., Dallaire, É., Dugat, J. and Aïcin, P.C. (1997), "Mechanical properties and durability of two industrial reactive powder concretes", *ACI Mater. J.*, **94**, 286-290.
- Chan, Y.W. and Chu, S.H. (2004), "Effect of silica fume on steel fiber bond characteristics in reactive powder concrete", *Cement Concrete Res.*, **34**(7), 1167-1172. <https://doi.org/10.1016/j.cemconres.2003.12.023>.
- Cheyrezy, M., Maret, V. and Frouin, L. (1995), "Microstructural analysis of RPC (reactive powder concrete)", *Cement Concrete Res.*, **25**(7), 1491-1500. [https://doi.org/10.1016/0008-8846\(95\)00143-Z](https://doi.org/10.1016/0008-8846(95)00143-Z).
- Cwirzen, A., Penttala, V. and Vornanen, C. (2008), "Reactive powder based concretes: Mechanical properties, durability and hybrid use with OPC", *Cement Concrete Res.*, **38**(10), 1217-1226. <https://doi.org/10.1016/j.cemconres.2008.03.013>.
- Dupont, D. and Vandewalle, L. (2005), "Distribution of steel fibers in rectangular sections", *Cement Concrete Compos.*, **27**(3), 391-398. <https://doi.org/10.1016/j.cemconcomp.2004.03.005>.
- Garas, V.Y., Kurtis, K.E. and Kahn, L.F. (2012), "Creep of UHPC in tension and compression: effect of thermal treatment", *Cement Concrete Compos.*, **34**(4), 493-502. <https://doi.org/10.1016/j.cemconcomp.2011.12.002>.
- Graybeal, B. and Baby, F. (2013), "Development of a direct tension test method for UHPFRC", *ACI Mater. J.*, **110**(2), 177-

- 186.
- Habel, K., Denarić, E. and Bruhwiler, E. (2007), "Experimental investigation of composite ultra-high performance fiber-reinforced concrete and conventional concrete members", *ACI Struct. J.*, **104**(1), 10-20.
- Hognestad, E. (1951), "Study of combined bending and axial load in reinforced concrete members", University of Illinois at Urbana Champaign, College of Engineering, Engineering Experiment Station.
- Hussein, L. and Amleh, L. (2015), "Structural behavior of ultra-high performance fiber reinforced concrete-normal strength concrete or high strength concrete composite members", *Constr. Build. Mater.*, **93**, 1105-1116. <https://doi.org/10.1016/j.conbuildmat.2015.05.030>.
- Jandaghi Alaei, F. and Karihaloo, B.L. (2003), "Retrofitting of reinforced concrete beams with CARDIFRC", *J. Compos. Constr.*, **7**, 174-186. [https://doi.org/10.1061/\(ASCE\)1090-0268\(2003\)7:3\(174\)](https://doi.org/10.1061/(ASCE)1090-0268(2003)7:3(174)).
- Kang, S.T., Lee, Y. and Park, Y.D. (2010), "Tensile fracture properties of an Ultra High Performance Fiber Reinforced Concrete (UHPFRC) with steel fiber", *Compos. Struct.*, **92**(1), 61-71. <https://doi.org/10.1016/j.compstruct.2009.06.012>.
- Kim, D.J., Park, S.H. and Ryu, G.S. (2011), "Comparative flexural behavior of hybrid ultra high performance fiber reinforced concrete with different macro fibers", *Constr. Build. Mater.*, **25**(11), 4144-4155. <https://doi.org/10.1016/j.conbuildmat.2011.04.051>.
- Lai, J. and Sun, W. (2010), "Dynamic tensile behaviour of reactive powder concrete by Hopkinson bar experiments and numerical simulation", *Comput. Concrete*, **7**(1), 83-86. <https://doi.org/10.12989/cac.2010.7.1.083>.
- Lamproulos, A.P., Paschalis, S.A., Tsioulou, O.T. and Dritsos, S.E. (2016), "Strengthening of reinforced concrete beams using ultra high performance fiber reinforced concrete (UHPFRC)", *Eng. Struct.*, **106**, 370-384. <https://doi.org/10.1016/j.engstruct.2015.10.042>.
- Mohammed, T.J., Abu Bakar, B.H. and Bunnori, N.M. (2015a), "Strengthening of reinforced concrete beams subjected to torsion with UHPFC composites", *Struct. Eng. Mech.*, **56**(1), 123-136. <https://doi.org/10.12989/sem.2015.56.1.123>.
- Mohammed, T.J., Abu Bakar, B.H., Bunnori, N.M. and Ibraheem, O.F. (2015b), "Finite element analysis of longitudinal reinforcement beams with UHPFC under torsion", *Comput. Concrete*, **16**(1), 1-16. <https://doi.org/10.12989/cac.2015.16.1.001>.
- Murthy, A.R., Karihaloo, B.L., Rani, P.V. and Priya, D.S. (2018), "Fatigue behaviour of damaged RC beams strengthened with ultra high performance fiber reinforced concrete", *Int. J. Fatig.*, **116**, 659-668. <https://doi.org/10.1016/j.ijfatigue.2018.06.046>.
- Murthy, R., Aravindan, M. and Ganesh, P. (2018), "Prediction of flexural behaviour of RC beams strengthened with ultra high performance fiber reinforced concrete", *Struct. Eng. Mech.*, **65**(3), 315-325. <https://doi.org/10.12989/sem.2018.65.3.315>.
- Nematzadeh, M. and Poorhosein, R. (2017), "Estimating properties of ultra-high performance fiber-reinforced concrete containing hybrid fibers using UPV", *Comput. Concrete*, **20**(4), 491-502. <https://doi.org/10.12989/cac.2017.20.4.491>.
- Noshiravani, T. and Brühwiler, E. (2013), "Experimental investigation on reinforced ultra-high-performance fiber-reinforced concrete composite beams subjected to combined bending and shear", *ACI Struct. J.*, **110**(2), 251-62.
- Park, S.H., Kim, D.J., Ryu, G.S. and Koh, K.T. (2012), "Tensile behavior of ultra high performance hybrid fiber reinforced concrete", *Cement Concrete Compos.*, **34**(2), 172-184. <https://doi.org/10.1016/j.cemconcomp.2011.09.009>.
- Poorhosein, R. and Nematzadeh, M. (2018), "Mechanical behavior of hybrid steel-PVA fibers reinforced reactive powder concrete", *Comput. Concrete*, **21**(2), 167-179. <https://doi.org/10.12989/cac.2018.21.2.167>.
- Qian, C.X. and Stroeven, P. (2000), "Development of hybrid polypropylene-steel fiber reinforced concrete", *Cement Concrete Res.*, **30**(1), 63-69. [https://doi.org/10.1016/S0008-8846\(99\)00202-1](https://doi.org/10.1016/S0008-8846(99)00202-1).
- Rahdar, H.A. and Ghalehnovi, M. (2016), "Post-cracking behavior of UHPC on the concrete members reinforced by steel rebar", *Comput. Concrete*, **18**(1), 139-154. <https://doi.org/10.12989/cac.2016.18.1.139>.
- Richard, P. and Cheyrezy, M. (1995), "Composition of reactive powder concretes", *Cement Concrete Res.*, **25**(7), 1501-1511. [https://doi.org/10.1016/0008-8846\(95\)00144-2](https://doi.org/10.1016/0008-8846(95)00144-2).
- Roux, N., Andrade, C. and Sanjuan, M.A. (1996), "Experimental study of durability of reactive powder concretes", *J. Mater. Civil Eng.*, **8**(1), 1-6.
- Safdar, M., Matsumoto, T. and Kakuma, K. (2016), "Flexural behavior of reinforced concrete beams repaired with ultra-high performance fiber reinforced concrete (UHPFRC)", *Compos. Struct.*, **157**, 448-460. <https://doi.org/10.1016/j.compstruct.2016.09.010>.
- Shi, C.J., Wang, D.H., Wu, L.M. and Wu, Z.M. (2015), "The hydration and microstructure of ultra high-strength concrete with cement-silica fume-slag binder", *Cement Concrete Compos.*, **61**, 44-52. <https://doi.org/10.1016/j.cemconcomp.2015.04.013>.
- Skazlic, M. and Bjegovic, D. (2009), "Toughness testing of ultra-high performance fiber reinforced concrete", *Mater. Struct.*, **42**(8), 1025-1038. <https://doi.org/10.1617/s11527-008-9441-3>.
- Tam, C.M., Tam, V.W.Y. and Ng, K.M. (2012), "Assessing drying shrinkage and water permeability of reactive powder concrete produced in Hong Kong", *Constr. Build. Mater.*, **26**(1), 79-89. <https://doi.org/10.1016/j.conbuildmat.2011.05.006>.
- Tanarlan, H.M. (2017), "Flexural strengthening of RC beams with prefabricated ultra high performance fiber reinforced concrete laminates", *Eng. Struct.*, **151**, 337-348. <https://doi.org/10.1016/j.engstruct.2017.08.048>.
- Tanarlan, H.M., Alver, N., Jahangiri, R., Yalçınkaya, Ç. and Yazıcı, H. (2017), "Flexural strengthening of RC beams using UHPFRC laminates: Bonding techniques and rebar addition", *Constr. Build. Mater.*, **155**, 45-55. <https://doi.org/10.1016/j.conbuildmat.2017.08.056>.
- Wang, C., Yang, C., Liu, F., Wan, C. and Pu, X. (2012), "Preparation of Ultra-High Performance Concrete with common technology and materials", *Cement Concrete Compos.*, **34**(4), 538-544. <https://doi.org/10.1016/j.cemconcomp.2011.11.005>.
- Wille, K., Kim, D. and Naaman, A.E. (2011a), "Strain-hardening UHP-FRC with low fiber contents", *Mater. Struct.*, **44**(3), 583-598. <https://doi.org/10.1617/s11527-010-9650-4>.
- Wille, K., Naaman, A.E. and Parra-Montesinos, G.J. (2011b), "Ultra-high performance concrete with compressive strength exceeding 150 MPa (22 ksi): a simpler way", *ACI Mater. J.*, **108**(1), 46-54.
- Williams, E.M., Graham, S.S., Akers, S.A., Reed, P.A. and Rushing, T.S. (2010), "Constitutive property behavior of an ultra-high-performance concrete with and without steel fibers", *Comput. Concrete*, **7**(2), 191-202. <https://doi.org/10.12989/cac.2010.7.2.191>.
- Yazıcı, H., Deniz, E. and Baradan, B. (2013), "The effect of autoclave pressure, temperature and duration time on mechanical properties of reactive powder concrete", *Constr. Build. Mater.*, **42**, 53-63. <https://doi.org/10.1016/j.conbuildmat.2013.01.003>.
- Yazıcı, H., Yardımcı, M.Y., Yigiter, H., Aydin, S. and Türkel, S. (2010), "Mechanical properties of reactive powder concrete containing high volumes of ground granulated blast furnace

- slag”, *Cement Concrete Compos.*, **32**(8), 639-648.
<https://doi.org/10.1016/j.cemconcomp.2010.07.005>.
- Zheng, W., Luo, B. and Wang Y. (2013), “Compressive and tensile properties of reactive powder concrete with steel fibers at elevated temperatures”, *Constr. Build. Mater.*, **41**, 844-851.
<https://doi.org/10.1016/j.conbuildmat.2012.12.066>.
- Zong-Cai, D., Daud, J.R. and Chang-Xing, Y. (2014), “Bonding between high strength rebar and reactive powder concrete”, *Comput. Concrete*, **13**(3), 411-421.
<https://doi.org/10.12989/cac.2014.13.3.411>.

SF